Environ. Sci. Technol. **2007**, *41,* 6762−6769

Assessing the Origin and Fate of Cr, Ni, Cu, Zn, Pb, and V in Industrial Polluted Soil by Combined Microspectroscopic Techniques and Bulk Extraction Methods

ROBERTO TERZANO,*,† MATTEO SPAGNUOLO,† BART VEKEMANS,‡ WOUT DE NOLF,‡ KOEN JANSSENS,‡ GERALD FALKENBERG,§ SAVERIO FIORE,|| AND PACIFICO RUGGIERO†

Dipartimento di Biologia e Chimica Agro-forestale ed Ambientale, Via Amendola 165/A, I-70126, University of Bari, Bari, Italy, Department of Chemistry, University of Antwerp, Universiteitsplein 1, B-2610, Wilrijk, Belgium, Istituto di Metodologie per l'Analisi Ambientale (I.M.A.A.), C.N.R, Contrada S. Loja, I-85050, Tito Scalo (PZ), Italy, and HASYLAB at DESY, Beamline L, Notkestraat 85, D-22603, Hamburg, Germany

The major geochemical forms of Cr, Ni, Cu, Zn, Pb, and V in a soil from an industrial polluted site in the south of Italy were determined by means of synchrotron X-ray microanalytical techniques such as coupled micro-X-ray fluorescence/micro-X-ray diffraction and micro-X-ray absorption near edge structure spectroscopy in combination with bulk extraction methods (sequential extraction procedures, EDTA extractions, and toxicity leaching characteristic procedure tests). Cr, Ni, Zn, and Cu were found in spinel-type geochemical forms (chromite, trevorite, franklinite, zincochromite, and cuprospinel) and often in association with magnetite and hematite. V was mainly present as V(V) associated with iron-oxides or in the form of volborthite [$Cu_3(OH)_2V_2O_7{\cdot}2H_2O$]. Pb was speciated as minium (Pb_3O_4), lanarkite [$Pb_2O(SO_4)$], and, in association with Cr(VI), as crocoite ($PbCrO_4$). In general, despite a high total concentration, metals appear to be speciated for the most part as rather insoluble geochemical forms. However, particular attention should be paid to Zn, Cu, V, and Pb that show non-negligible mobilizable fractions. On the basis of the geochemical forms identified, among others, two major former industrial activities were tentatively ascribed as being responsible for the observed major pollution: polyvinyl chloride and cement−asbestos productions.

Introduction

It is commonly recognized that soil is the major sink for heavy metal (HM) contaminants released into the environment by anthropogenic activities and that the mobility, bioavailability, and toxicity of metals strongly depend on their solubility and therefore on their geochemical forms. The correct identification of HM chemical forms in soil is therefore of paramount relevance for a proper risk assessment and for the formulation of effective remediation strategies.

Gathering this type of information presents considerable analytical difficulties since the contamination may be extremely heterogeneous and the sites may contain large quantities of anthropogenic materials. In addition, many former industrial sites have been used for various manufacturing processes, often over several decades, and it is rare for only one contaminant to be present. Therefore, the methods developed for the analysis of conventional soils may not always prove to be appropriate for soils sampled in industrial sites.

In recent years, the development of new analytical methods exploiting high-energy and high-intensity synchrotron generated X-rays has provided soil scientists with new powerful tools for shedding light on HM speciation in soil. In particular, given the large number of different phases in soils and their complex and heterogeneous distribution, the use of synchrotron X-ray microbeam techniques can resolve the metal bearing phases at the micrometer (or submicrometer) level, thus allowing for a more selective and direct approach to HM speciation. These techniques also have the advantage of reducing analytical artifacts caused by extensive sample manipulations. Even if soil is a matrix that is heterogeneous down to the nanometer scale, soil components are often grouped into micrometer-sized aggregates, making the micrometer scale of resolution appropriate for speciation investigations (*1*).

Microscopic synchrotron radiation (SR) tools have been successfully used to characterize metals in contaminated soils and sediments (*2*−*9*) and include micro-X-ray fluorescence (μ-XRF), micro-X-ray diffraction (μ-XRD), and micro-X-ray absorption spectroscopy [μ-XAS: X-ray absorption near edge structure (XANES) spectroscopy and extended X-ray absorption fine structure (EXAFS) spectroscopy].

Some of these studies aimed also at reliably extending the information obtained from microscopic portions of soil samples to a higher length bulk scale. One of the most successful methods employed to accomplish this extrapolation has been to combine μ-EXAFS with bulk EXAFS measurements and to interpret the bulk EXAFS spectra in light of the more easily manageable information obtained from μ-EXAFS analyses (*6*−*9*). The only drawbacks of this EXAFS-based method, besides the difficulty in analyzing data, are practical ones, such as the need of a light source with a very high brightness, which can be only provided by third generation synchrotron facilities, and the availability of an extensive spectral database obtained by analyzing a number of reference compounds (both natural and synthetic) including all the metal forms most likely to be present in the soil under investigation. For these reasons, this method has been generally adopted to extensively study only one or, in any case, just a few metal pollutants in soil and sediments (*10*).

A more practical approach toward bulk metal speciation in soil involves single or sequential extraction procedures. In principle, this approach allows for the identification and quantification of as many metal forms as there are extraction steps using chemical reagents of different binding strengths and metal specificities (*4*, *11*). However, these procedures have many pitfalls such as a lack of selectivity of reagents, incomplete dissolution of target phases, readsorption and

* Corresponding author phone: +39 080 5442847; fax: +39 080 5442850; e-mail: r.terzano@agr.uniba.it.
† University of Bari.
‡ University of Antwerp.
§ HASYLAB at DESY.
|| I.M.A.A.

10.1021/es070260h CCC: $37.00

Published on Web 08/29/2007

redistribution phenomena, and possible modification of redox sensitive elements (*12*).

In this study, we used a combination of microanalytical techniques exploiting synchrotron generated X-rays as well as different bulk extraction methods to assess the geochemical forms and chemical behavior of various HM pollutants (Cr, V, Pb, Ni, Cu, and Zn) in a soil from an industrial polluted site in the south of Italy. The need for an urgent and detailed characterization of metal pollution in this site arose from particular concerns about the mobility of the metals at this site, located in a river basin with quite shallow groundwater and surrounded by widespread agricultural activities.

μ-XRF was used to localize metals in soil thin sections and to find correlations among different elements. Simultaneously, μ-XRD patterns were collected to obtain information about the minerals to which HM was associated. The simultaneous acquisition of μ-XRF and μ-XRD data was possible by collecting XRD patterns in transmission mode rather than in reflection mode (*1*). This could be done by using an X-ray focusing system ensuring a high flux, and by preparing the soil thin sections with a suitable X-ray transparent support.

In addition, μ-XANES spectroscopy point analyses were performed to determine the oxidation state of pollutants such as Cr and V and to better define the association of various other metals with minerals, by comparison with selected mineral standards. The information revealed by these SR analyses allowed for HM speciation at the microscopic level.

All results emerging from both the microscopic (X-ray-based) and the macroscopic (bulk extraction-based) investigations were combined and employed to identify the possible former sources of metal pollution and to predict the fate of these elements in soil.

Materials and Methods

Soil. Superficial soil samples were collected from 0 to 30 cm depth on a sampling area of 60 ha and at a distance of 100 m on a square grid basis. Soil samples were air-dried and sieved at 2 mm. Details about the sampled site are reported in the Supporting Information.

The total trace metal concentration was measured using HNO_3/HCl/HF sample microwave assisted digestion (EPA Method 3052). The solutions were analyzed using inductively coupled plasma atomic emission spectroscopy (ICP-AES; Trace Scan, Thermo Jarrel Ash). The most heavily contaminated sample was then selected for more detailed experiments and is the object of the present study.

Cr(VI) was quantified using both alkaline (EPA Method 3060A) and acid (*13*) extractions followed by spectrophotometric determination with diphenylcarbazide (EPA Method 7196A).

The major elemental composition of the soil was determined by X-ray fluorescence (XRF) analysis using a Philips PW2400 spectrometer. Powders were fused with lithium tetraborate at 1:10 w/w ratio, and quantitative determination was obtained against about 30 international geologic standards.

Bulk semiquantitative mineralogy of the 2 mm fraction as well as of the <2 μm fraction was determined by powder X-ray diffraction using a Rigaku D/MAX-2200/PC diffractometer operating at 40 kV and 30 mA with Cu$-$ Kα radiation and a flat graphite monochromator. Various soil characteristics such as texture, pH, EC, organic C, organic matter (OM), total N, C/N, and exchangeable cations were also determined.

Sample Preparation for Microscopic Analyses. The soil sample was embedded in acrylic resin (LR-White, SPI Supplies), hardened, cut, mounted on ultrapure fused quartz slides (900 μm thickness, SPI Supplies), and polished into thin sections of 20 and 60 μm. A total of seven thin sections was prepared from three different blocks and analyzed.

Microscopic Investigations. Thin sections were sputter coated with a carbon layer and preliminarily examined by SEM using a JEOL JSM 6300 microscope. The backscattered electron imaging mode was used to locate areas with high concentrations of HM. The coordinates of these areas, relative to a reference point marked by means of a diamond edge on the sample, were accurately recorded (within a precision of 1 μm) and were used to find them when performing the microanalytical investigations with SR X-rays.

Synchrotron X-ray microscopic measurements (μ-XRF, μ-XRD, and μ-XANES) were performed on Beamline L at the Hamburger Synchrotronstrahlungslabor (HASYLAB, Hamburg, Germany). A description of the experimental setup adopted and all the analytical details are reported in the Supporting Information.

All the thin sections were further extensively analyzed by EPXMA (electron probe X-ray micro-analysis) to have an additional overview of the samples to better evaluate the synchrotron X-ray microscopic data (data not shown).

Bulk Extraction Methods. Sequential extractions were carried out following a modified Tessier et al. procedure (*14*) and the BCR scheme (*15*). Details about the extraction procedures adopted are reported in the Supporting Information.

EDTA extractions were performed on soil samples to assess the metals' available fraction (*16*). Fifty milliliters of a 50 mM EDTA solution was added to 0.5 g of soil. After adjusting the pH to 7.0 by adding a few drops of NaOH solution (10 M), the mixtures were shaken for 48 h by means of a reciprocal shaker. TCLP (toxicity leaching characteristic procedure) tests were carried out following U.S. EPA protocol (EPA Method 1311). All the extracts, after centrifugation and filtration at 0.45 μm, were analyzed by means of ICP-AES (Trace Scan, Thermo Jarrel Ash). All experiments were conducted in triplicate.

Results and Discussion

Mineralogical and Chemical Characterization. The soil mineralogical composition is reported in Table S1 (Supporting Information). The soil under investigation is a sandy loam soil (USDA) with a high percentage of skeleton (49%), an alkaline pH (8.8), and a very low content of organic matter (0.64%) and phyllosilicates. It is rich in Fe minerals and shows a very high calcite and Ca content.

The soil chemical composition including the total trace metal concentration is reported in Table 1. In particular, this soil shows a high content of different HM: Cr, V, Zn, Cu, Ni, and Pb. In Italy, total concentrations of contaminant metals and metalloids in soil are generally compared with guideline levels issued by the Italian Environmental Ministry (D.Lgs. 152/2006). All the previously reported elements significantly exceed the threshold trigger values imposed by this law. Also, Cr(VI) is above the reference limits. The amount of metals determined after acid digestion with HNO_3 or including HF was exactly the same. Therefore, metals were not expected to be sequestered in siliceous minerals.

From the XRD pattern collected on the soil powder (total and <2 μm), no mineral phase directly attributable to pure HM minerals was detectable. Diffraction peaks attributable to hematite and magnetite were clearly visible. Some of the characteristics of the soil (high pH, high content of calcite and iron oxides) and the amount and variety of metal pollutants, as compared to the geological and chemical characteristics of native soils collected in the same area, suggest that this soil was highly impacted by anthropogenic activities.

Metal Geochemical Forms Determined by Combined μ-XRF/μ-XRD and μ-XANES. Several microareas on different soil thin sections were analyzed by means of combined synchrotron μ-XRF/μ-XRD and by extensive SEM-EDX analy-

TABLE 1. Soil Chemical Composition for Major and Trace Elements and Microscopically Identified Metal Geochemical Forms

major elements	percent	trace elements	concentration (μg/g)	microscopically identified phases
SiO_2[a]	40.1	Crtot[b]	352 ± 37	chromite, zincochromite, sorbed on hematite
TiO_2[a]	0.6	Cr(VI)alk[b]	5.1 ± 0.9	crocoite
Al_2O_3[a]	9.8	Cr(VI)ac[b]	12 ± 2	
Fe_2O_3[a]	16.4	Zn[b]	1196 ± 53	franklinite, zincochromite, sorbed on hematite
MnO[a]	0.3	Ni[b]	394 ± 17	trevorite, sorbed on hematite
MgO[a]	1.4	Cu[b]	449 ± 8	cuprospinel, volborthite, sorbed on hematite
CaO[a]	18.1	Pb[b]	1080 ± 150	minium, lanarkite, crocoite
Na_2O[a]	0.6	V[b]	1688 ± 24	volborthite, V(V) sorbed on hematite
K_2O[a]	1.1	Ba[b]	445 ± 12	barite
L.O.I.	11.6			

[a] Determined by XRF. [b] Determined by ICP-AES; alk: alkaline extraction and ac: acidic extraction.

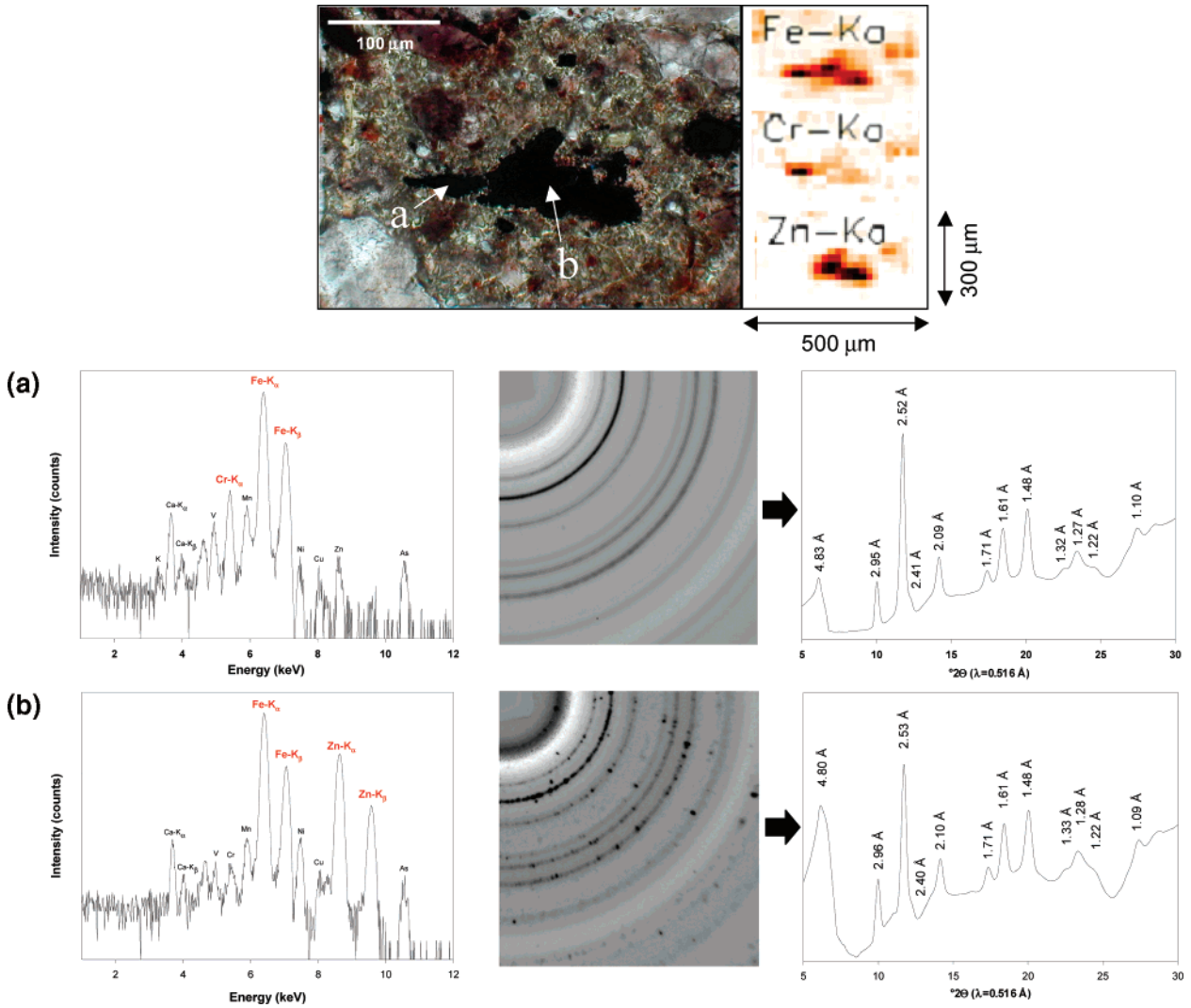

FIGURE 1. Micrograph with the corresponding μ-XRF distribution maps (for Fe, Cr, and Zn) of a microscopic area on a soil thin section analyzed by combined μ-XRF/μ-XRD. Darker pixels correspond to relative higher concentrations of the element. μ-XRF spectra and μ-XRD images (also converted into 1-D diffraction patterns) were collected in points a and b (indicated by the arrows in the micrograph). *d*-Spacing values corresponding to diffraction peaks are also shown in the 1-D diffractogram. Reported *d*-spacings are characteristic of spinel-type minerals: (a) chromite and/or magnetite and (b) franklinite and/or magnetite.

ses; therefore, all the reported data may represent, with a good deal of confidence, the geochemical forms most frequently observed at the microscopic level in the soil sample. However, as in any other microanalytical approach, the data obtained is derived only from infinitesimal portions of the whole sample, but it is at this microscopic level that the most relevant information on metal speciation originates. More general information on the bulk behavior of metals has been assessed by extraction methods, as reported in the following section.

μ-XRF maps were used to find correlations among elements in the sample, pinpointing areas of interest after which μ-XRD data were exploited to identify crystalline mineral forms in which metals were present in a specific form or soil minerals on which metals were sorbed.

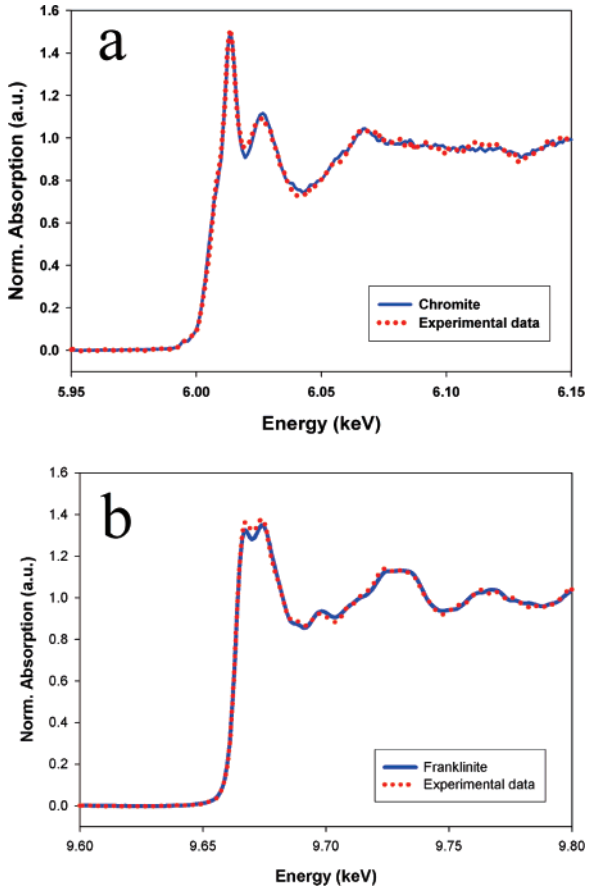

FIGURE 2. (a) Cr μ-XANES spectrum collected in point a of Figure 1. (b) Zn μ-XANES spectrum collected in point b of Figure 1. Experimental spectra are shown overlapped with the spectra of selected Cr and Zn standards (chromite and franklinite, respectively).

Cr, in the same way as Zn, was in most cases found to be related to Fe minerals. Figure 1 shows a picture of a microscopic area analyzed on a thin section and the corresponding μ-XRF 2-D maps for Fe, Cr, and Zn. From these maps, relations among these elements are easily visible, and, for example, in the case of Cr, the relation between Cr and Fe is evidenced in the μ-XRF spectrum collected in point a and reported in Figure 1a. μ-XRD analysis performed on the same point revealed the occurrence of a spinel-type iron-mineral as it can be deduced from the 2-D and 1-D diffraction patterns reported in Figure 1a. However, from this information, it is only possible to infer that Cr is related to an iron-oxide spinel-type mineral, without knowing if this metal is in the structure of the mineral (e.g., chromite, $FeCr_2O_4$) or just somehow sorbed to it (e.g., Cr sorbed to magnetite, Fe_3O_4). In fact, chromite and magnetite show almost the same diffraction pattern. To solve this ambiguity, Cr μ-XANES spectra were collected in the same point and compared with the spectra obtained for selected Cr standards. As shown in Figure 2a, the experimental Cr-XANES data are exactly fitted by the spectrum collected for a chromite standard. Therefore, in this particle, Cr was in the form of chromite. A similar mineral form was found for Zn (Figure 1b). In the case of Zn, μ-XANES data confirmed the presence of franklinite ($ZnFe_2O_4$, Figure 2b).

Cr and Zn were also found in the form of zincochromite ($ZnCr_2O_4$), and geochemical forms with analogous mineralogical structures were also detected for Ni and Cu. For these metals, minerals such as trevorite ($NiFe_2O_4$) and cuprospinel ($CuFe_2O_4$) were identified (data not shown).

Cr, Zn, Cu, Ni, and V were also frequently found associated with hematite (Fe_2O_3). An example of this correlation is reported in Figure 3.

Vanadium μ-XANES experiments evidenced the presence of V(V) throughout all investigated samples. For example, Figure 4a shows the V-XANES spectrum collected in the point indicated in Figure 3 and analyzed also with μ-XRF and μ-XRD. The spectra of vanadium oxide standards at different oxidation states are also reported. The position and intensity of the pre-edge peak as well as the positive shift of the main absorption edge measured at an absorption equal to 0.5 (as indicated by refs *17* and *18*) suggest that in the sample, vanadium is mostly present as V(V). In general, V was frequently found associated with iron-oxides, in particular, with hematite and magnetite.

In the case of hematite, metals were probably sorbed on this mineral, even if the microscopic techniques adopted could not clarify this aspect. μ-EXAFS measurements could have better solved the nature of metal−mineral interactions. However, at the beamline where the experiments were carried out, the brightness was not high enough to obtain clearly interpretable μ-EXAFS data. Nevertheless, as will be discussed in the next section, additional information coming from bulk extraction methods could be used to evaluate the role and extent of these metal−mineral interactions.

Volborthite [$Cu_3(OH)_2V_2O_7{\cdot}2H_2O$], a mineral phase containing V and Cu, was also frequently found in the investigated samples (Figure S2, Supporting Information). A very interesting speciation was found for Pb. Pb was often found in large aggregates of hundreds of micrometers in correlation with Ba, S (detectable by EPXMA analysis), and Cr (Figure 5). Cr in these aggregates was found in the form of Cr(VI) by μ-XANES analysis as reported in the spectrum shown in Figure 4b, where the characteristic pre-edge peak of Cr(VI) below the main absorption edge of Cr is easily visible. μ-XRD analyses revealed a very complex diffraction pattern made up of the contribution of different mineral phases. Minerals contributing to the diffractogram shown in Figure 5 are minium (Pb_3O_4), lanarkite [$Pb_2O(SO_4)$], barite ($BaSO_4$), and crocoite ($PbCrO_4$) (further details are reported in the Supporting Information, Table S2). As a summary, an overview of all the main mineral phases microscopically identified for the different HM is reported in Table 1.

Sequential Extractions and Leaching Tests. Results from the sequential extraction procedure are reported in Figure S3 (Supporting Information). Cr was almost completely found in the residual fraction (93%), and according to the speciation determined with the microanalytical approach, it should be in the structure of chromite ($FeCr_2O_4$) minerals. The consideration previously made on the total concentrations determined with or without using HF can exclude the presence of Cr inside siliceous or aluminosiliceous minerals. Cr(VI) was encountered mainly in the form of crocoite ($PbCrO_4$). This observation is also supported by the different value of Cr(VI) extractable in alkaline or in acidic conditions. It is well-known that hardly soluble chromates such as $BaCrO_4$ and $PbCrO_4$ are more easily solubilized in acidic conditions. This might explain the higher value (12 μg/g) obtained after acidic extraction (Table 1). The small amount of Cr extractable in reducing conditions (5%) could be attributed to Cr associated with hematite (Fe_2O_3) (most likely sorbed as an inner sphere complex (*19*)). Also, EDTA extraction is capable of extracting only a small amount of Cr (6%). In general, the extraction procedure adopted for the assessment of the reducible fraction can easily dissolve only amorphous iron oxides, while crystalline iron oxides are expected to remain stable (*14*, *20*). As well, EDTA can extract only metals sorbed on mineral surfaces and promote the dissolution of poorly crystalline phases (*16*).

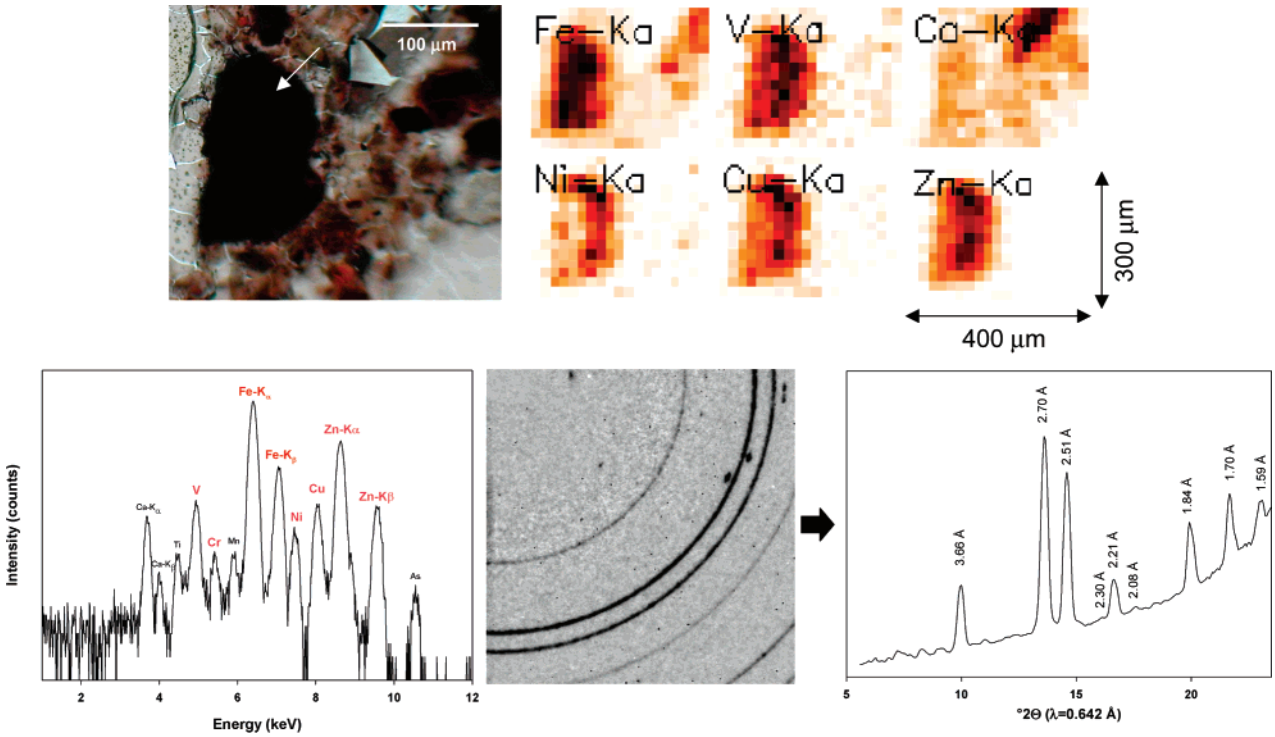

FIGURE 3. Micrograph with the corresponding μ-XRF distribution-maps (for Fe, V, Ca, Ni, Cu, and Zn) of a microscopic area on a soil thin section analyzed by combined μ-XRF/μ-XRD. Darker pixels correspond to relative higher concentrations of the element. μ-XRF spectrum and μ-XRD image (also converted into a 1-D diffraction pattern) were collected in the point indicated by the arrow in the micrograph. *d*-Spacing values corresponding to the diffraction peaks are also shown in the 1-D diffractogram. Reported *d*-spacings are characteristic of hematite.

A similar behavior was observed for Ni, where 77% of it was found in the residual fraction. According to microscopic observations, Ni can be in the form of trevorite ($NiFe_2O_4$). The reducible fraction (16%) can be again attributed to Ni sorbed on hematite or on amorphous iron-minerals. The small oxidizable fraction observed for both Cr (2%) and Ni (5%), usually attributed to metals linked to organic matter, can be explained by the very low content of soil OM (6.4 g/kg). EDTA extractable Ni was also very low (8%). According to these data, a good agreement was found between the microscopic speciation and the macroscopic behavior of Cr and Ni.

Pb was mainly found in the reducible fraction (60%), which is usually attributed to metals associated with iron- or manganese-oxides. However, from microscopic analyses, this kind of association was rarely found, even if several iron-oxides were studied in detail. Therefore, for Pb, an interpretation of the results based only on the indications of the sequential extractions would have probably led to an incorrect metal speciation. The increased solubility in reducing conditions could be, instead, partly attributed to minium (Pb_3O_4). Minium is an insoluble mineral, but reducing conditions could favor the reduction of Pb(IV) to Pb(II), thus increasing its solubility. Another contribution to the reducible fraction could have been given by Pb sulfates that, as it is known, can be dissolved in acidic conditions but tend to redistribute on iron-oxides (*12*). Moreover, the high soil carbonate content might have prevented the dissolution of acid-soluble phases, thus leading to a higher Pb distribution in the reducible fraction. The residual fraction (34%) could include the identified $PbCrO_4$ and partially insolubilized minium. Also for Pb, the oxidizable fraction was very low (4%). The EDTA extractable fraction was quite high (27%), thus creating, differently from Cr and Ni, more concern for Pb availability.

Vanadium was equally distributed between the reducible (40%) and the residual fractions (43%). Microanalysis always showed a relation between this element and iron-oxides, in particular, hematite and magnetite. μ-XANES measurements showed V mainly in the form of V(V). The reducible fraction could be attributed to V bound to the surface of iron-oxides or linked to poorly crystallized iron-minerals, while the residual can be ascribed to V more deeply buried in the structure of crystalline hematite or magnetite as well as to volborthite [$Cu_3(OH)_2V_2O_7{\cdot}2H_2O$]. A significant fraction (16%) of the total V was found in the oxidizable fraction, and 21% was extracted by EDTA. All the metals discussed up to this point did not show appreciable amounts of exchangeable or acid-soluble fractions. This aspect suggests a very low mobility and, therefore, a reduced potential for environmental risk.

For copper and zinc, a different behavior was observed. Zinc showed a 50% residual fraction attributable to franklinite ($ZnFe_2O_4$) and zincochromite ($ZnCr_2O_4$). The reducible fraction (28%) can be ascribed to Zn sorbed on hematite or on poorly crystalline iron-minerals. However, more labile Zn forms were also present (most probably in the form of carbonates) since the acid extractable fraction was 14%. In fact, the amount of carbonate in soil was very high (46%). Only very small Zn percentages, 3 and 5%, were found in the exchangeable and oxidizable fraction, respectively. About 30% of total Zn could be leached by EDTA extraction. Therefore, Zn showed a non-negligible potential mobility and availability.

Cu, besides the microscopically identified forms of cuprospinel ($CuFe_2O_4$) and volborthite [$Cu_3(OH)_2V_2O_7{\cdot}2H_2O$], which may account for the determined residual fraction (43%), also showed significant contributions from all the other four more available fractions: oxidizable 20%, reducible 17%, exchangeable 12%, and acid soluble 8%. The reducible fraction can be ascribed, as for the other metals, to Cu sorbed on hematite, but for this element, the fraction associated with OM is also significant. It is well-known that among all the investigated metals, Cu presents the highest affinity for

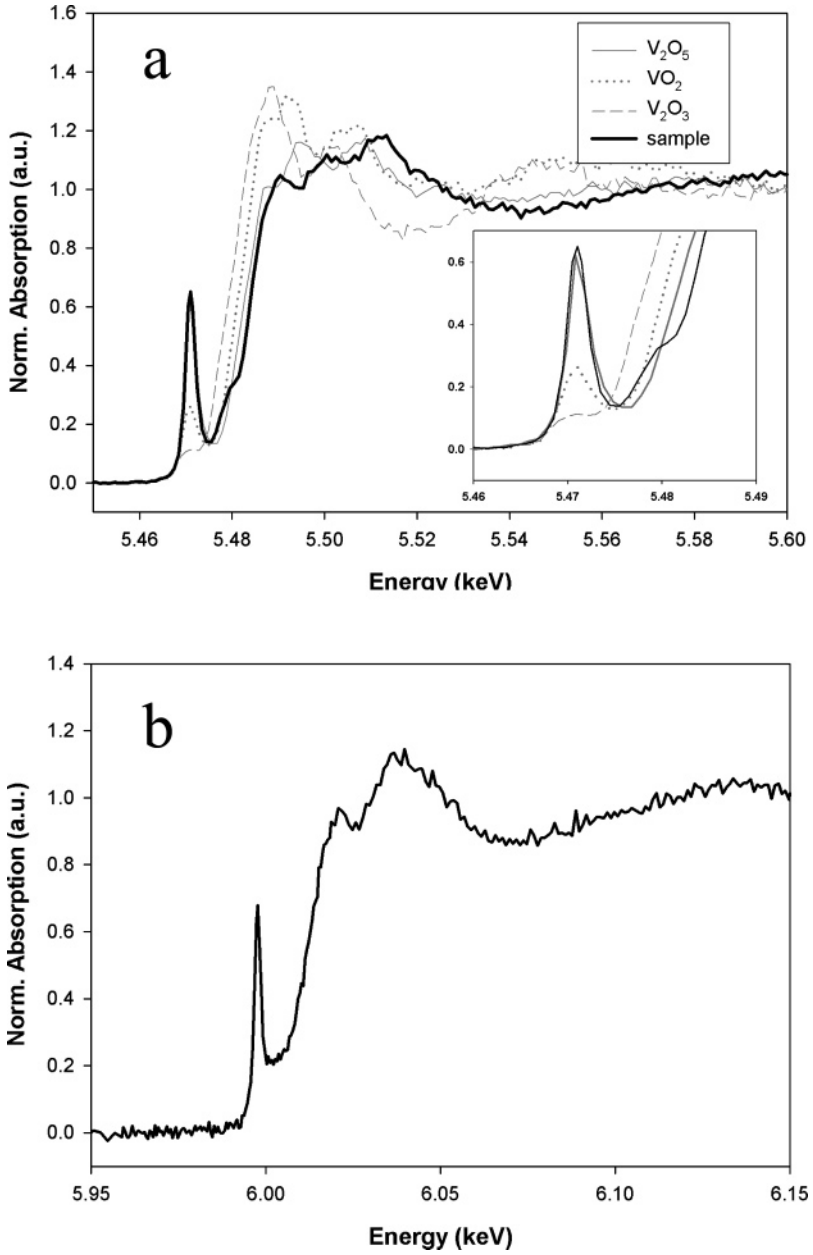

FIGURE 4. (a) V μ-XANES spectrum collected in the point indicated by the arrow in Figure 3. Spectra of vanadium oxide standards at different oxidation states are also reported. An expanded region of the spectra is shown in the bottom right corner. (b) Cr μ-XANES spectrum collected in the point indicated by the arrow in Figure 5.

OM (*21*). Also, the more labile fractions (exchangeable and acid soluble) were quite high with an overall value of 20%. The higher potential mobility of Cu was confirmed by EDTA extraction, which caused the solubilization of 39% of total Cu.

The BCR procedure was also adopted to assess the distribution of metals in different operative pools. The obtained results were almost identical to those reported previously with the exception of the oxidizable fraction, which was generally found to be higher with the BCR extraction method, in particular, for Cu and Pb (*12*). All metals passed the TCLP test, showing a very low mobility in acidic conditions. However, the soil alkaline pH certainly contributed to prevent metals from leaching.

Origin and Fate of Metal Pollutants. The metal geochemical forms determined by using the combined spectromicroscopic techniques were compared with the geochemical characteristics of the site under investigation, and the industrial activities once operating on this site (from the 1960s to the 1980s) were reviewed to allow the attribution of the possible sources of pollution.

During this period, several industrial activities with extremely different productions followed one another in the area under investigation. However, from our survey, only two major former industrial activities could be ascribed as responsible for the observed major pollution: PVC (polyvinyl chloride) production and cement−asbestos products manufacture.

The origin of V(V) could be ascribed to discarded spent catalysts (V_2O_5) employed in the oxidation of orthoxylene or naphthalene for the production of phtalic anhydride used for making plasticizers for PVC manufacture. $PbCrO_4$, $PbSO_4$, and minium (together with $BaSO_4$) were well-known pigments used as dyes in PVC production. Moreover, Pb salts such as tribasic lead sulfate were also frequently used as stabilizers in PVC manufacture.

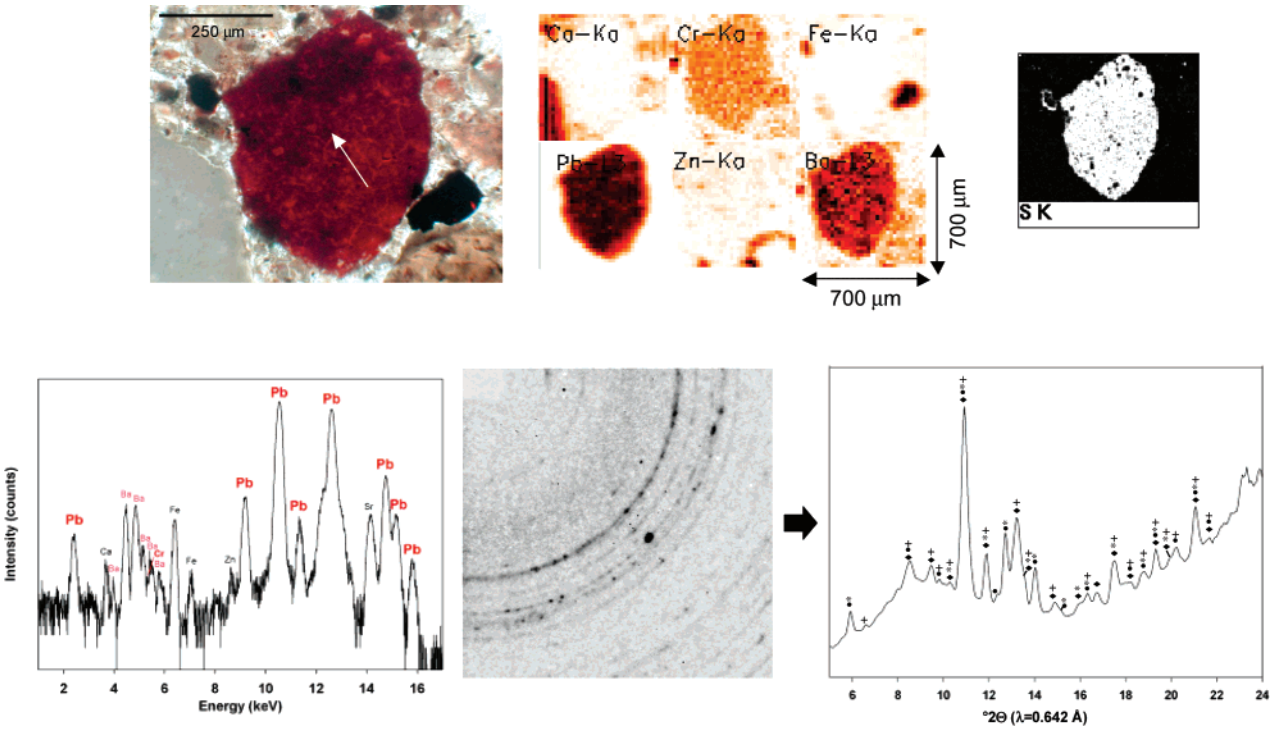

FIGURE 5. Micrograph with the corresponding μ-XRF distribution maps (for Ca, Cr, Fe, Pb, Zn, and Ba) of a microscopic area on a soil thin section analyzed by combined μ-XRF/μ-XRD. Darker pixels correspond to relative higher concentrations of the element. Same area was analyzed by EPXMA for S distribution (brighter pixels correspond to higher concentrations of the element). μ-XRF spectrum and μ-XRD image (also converted into a 1-D diffraction pattern) were collected in the point indicated by the arrow in the micrograph. Attribution of the diffraction peaks is also reported in the 1-D diffractogram: ♦, barite; +, crocoite; *, minium; and ●, lanarkite. Details on peak attributions are reported in Table S2 (Supporting Information).

Cr, Ni, Zn, and Cu were highly present in spinel-type geochemical forms (chromite, trevorite, franklinite, cuprospinel, etc.) and were often in association with magnetite and hematite. These minerals often can be found in natural soils; nevertheless, natural soils collected around the industrial area usually show an amount of crystalline iron-oxides ranging only from 0.1 to 2.0%, most of which is represented by goethite rather than magnetite, hematite, or other spinel-type forms. In the investigated soil, an anthropogenic origin therefore can be attributed to these geochemical forms. These minerals are typically produced at high temperatures during processes involving iron-minerals. Such temperatures can be reached during clinker production for Portland cement manufacture. The high Ca content, alkaline pH, soil texture, as well as some SEM observations (not shown) all indicate the presence of cementitious materials. In addition, asbestos fibers were also found in this soil by SEM observations (Figure S4, Supporting Information). Therefore, this type of pollution can be most probably ascribed to cement−asbestos products manufactore.

From the data presented in this research, despite a high total concentration, most of the HM appear to be speciated in rather insoluble geochemical forms. Therefore, the environmental danger connected with their presence in the investigated soil is estimated to be much lower than expected. However, particular attention should be paid to Zn, Cu, V, and Pb that show non-negligible mobilizable fractions, as evidenced by EDTA extractions.

In conclusion, the microscopic techniques adopted proved to be very effective to identify, in the case of rather unusual mineral phases, the more stable metal forms (as evidenced for Cr, Ni, Pb, and V), while the more labile ones were better assessed with the help of bulk extraction methods (as shown for Zn and Cu).

Acknowledgments

This research was financed by the MIUR (COFIN 2005) Project "Innovative Chemical, Physical, and Biological Methods to Characterize and Remediate Soils Polluted by Heavy Metals (MICROS)" and by the IMAA-CNR Project "Elemental Mobility Geochemical Map in Basilicata, Italy". Synchrotron experiments at HASYLAB were financially supported by the European Community−Research Infrastructure Action under the FP6 "Structuring the European Research Area" Program (Integrating Activity on Synchrotron and Free Electron Laser Science; Contract RII3-CT-2004-506008).

Supporting Information Available

Details concerning site description, sequential extraction procedures, and synchrotron X-ray microscopic analyses. Table reporting soil mineral composition, figure on volborthite identification, table giving details on attribution of diffraction peaks shown in Figure 5, SEM micrographs of asbestos fibers, and graph schematizing results from sequential extraction procedures. This material is available free of charge via the Internet at http://pubs.acs.org.

Literature Cited

(1) Manceau, A.; Marcus, M. A.; Tamura, N. Quantitative speciation of heavy metals in soils and sediments by synchrotron X-ray techniques. In *Applications of Synchrotron Radiation in Low-Temperature Geochemistry and Environmental Science*; Fenter, P., Sturchio, N. C., Eds.; Reviews in Mineralogy and Geochemistry; Mineralogical Society of America: Washington, DC, 2002; Vol. 49, pp 341−428.

(2) Isaure, M. P.; Laboudigue, A.; Manceau, A.; Sarret, G.; Tiffreau, C.; Trocellier, P.; Lamble, G.; Hazemann, J. L.; Chateigner, D. Quantitative Zn speciation in a contaminated dredged sediment by μ-PIXE, μ-SXRF, EXAFS spectroscopy, and principal component analysis. *Geochim. Cosmochim. Acta* **2002**, *66*, 1549−1567.

(3) Bernaus, A.; Gaona, X.; Esbrì, J. M.; Higueras, P.; Falkenberg, G.; Valiente, M. Microprobe techniques for speciation analysis and geochemical characterization of mine environments: The mercury district of Almadén in Spain. *Environ. Sci. Technol.* **2006**, *40*, 4090−4095.
(4) Kirpichtchikova, T. A.; Manceau, A.; Spadini, L.; Panfili, F.; Marcus, M. A.; Jacquet, T. Speciation and solubility of heavy metals in contaminated soil using X-ray microfluorescence, EXAFS spectroscopy, chemical extraction, and thermodynamic modeling. *Geochim. Cosmochim. Acta* **2006**, *70*, 2163−2190.
(5) Ryser, A. L.; Strawn, D. G.; Marcus, M. A.; Fakra, S.; Johnson-Maynard, J. L.; Möller, G. Microscopically focused synchrotron X-ray investigation of selenium speciation in soils developing on reclaimed mine lands. *Environ. Sci. Technol.* **2006**, *40*, 462−467.
(6) Roberts, D. R.; Scheinost, A. C.; Sparks, D. L. Zinc speciation in a smelter-contaminated soil profile using bulk and microspectroscopic techniques. *Environ. Sci. Technol.* **2002**, *36*, 1742−1750.
(7) Isaure, M. P.; Manceau, A.; Geoffroy, N.; Laboudigue, A.; Tamura, N.; Marcus, M. A. Zinc mobility and speciation in soil covered by contaminated dredged sediment using micrometer-scale and bulk-averaging X-ray fluorescence, absorption, and diffraction techniques. *Geochim. Cosmochim. Acta* **2005**, *69*, 1173−1198.
(8) Panfili, F.; Manceau, A.; Sarret, G.; Spadini, L.; Kirpichtchikova, T.; Bert, V.; Laboudigue, A.; Marcus, M. A.; Ahamdach, N.; Libert, M.-F. The effect of phytostabilization on Zn speciation in a dredged contaminated sediment using scanning electron microscopy, X-ray fluorescence, EXAFS spectroscopy, and principal component analysis. *Geochim. Cosmochim. Acta* **2005**, *69*, 2265−2284.
(9) Manceau, A.; Lanson, B.; Schlegel, M. L.; Hargé, J. C.; Musso, M.; Eybert-Bérard, L.; Hazemann, J.-L.; Chateigner, D.; Lamble, G. M. Quantitative speciation in smelter-contaminated soils by EXAFS spectroscopy. *Am. J. Sci.* **2000**, *300*, 289−343.
(10) Roberts, D.; Nachtegaal, M.; Sparks, D. L. Speciation of metals in soils. In *Chemical Processes in Soils*; Tabatabai, M. A., Sparks, D. L., Eds.; Soil Science Society of America Book Series: Madison, WI, 2005; Vol. 8, pp 619−654.
(11) Scheinost, A. C.; Kretzschmar, R.; Pfister, S. Combining selective sequential extractions, X-ray absorption spectroscopy, and principal component analysis for quantitative zinc speciation in soil. *Environ. Sci. Technol.* **2002**, *36*, 5021−5028.
(12) Gleyzes, C.; Tellier, S.; Astruc, M. Fractionation studies of trace elements in contaminated soils and sediments: A review of sequential extraction procedures. *TrAC, Trends Anal. Chem.* **2002**, *21*, 451−467.
(13) IRSA-CNR. Metodi analitici per i fanghi. Vol. 3. Parametri chimico-fisici. *Quad. Ist. Ric. Acque*, **1986**, *64*, 16.
(14) Tessier, A.; Campbell, P. G. C.; Bisson, M. Sequential extraction procedure for the speciation of particulate trace metals. *Anal. Chem.* **1979**, *51*, 844.
(15) Rauret, G.; López-Sánchez, J.-F.; Sahuquillo, A.; Barahona, E.; Lachica, M.; Ure, A. M.; Davidson, C. M.; Gomez, A.; Luck, D.; Bacon, J.; Yli-Halla, M.; Muntau, H.; Quevauviller, P. Application of a modified BCR sequential extraction (three-step) procedure for the determination of extractable metal contents in a sewage sludge amended soil reference material (CRM 483), complemented by a three year stability study of acetic acid and EDTA extractable metal content. *J. Environ. Monit.* **2000**, 228−233.
(16) Garrabrants, A. C.; Kosson, D. S. Use of chelating agent to determine the metal availability for leaching from soils and wastes. *Waste Manage.* **2000**, *20*, 155−165.
(17) Chaurand, P.; Rose, J.; Briois, V.; Olivi, L.; Hazemannd, J.-L.; Proux, O.; Domas, J.; Bottero, J. Y. Environmental impacts of steel slag reused in road construction: A crystallographic and molecular (XANES) approach. *J. Hazard. Mater.* **2007**, *139*, 537−542.
(18) McKeown, D. A.; Muller, I. S.; Matlack, K. S.; Pegg, I. L. X-ray absorption studies of vanadium valence and local environment in borosilicate waste glasses using vanadium sulfide, silicate, and oxide standards. *J. Non-Cryst. Solids* **2002**, *298*, 160−175.
(19) Doelsch, E.; Basile-Doelsch, I.; Rose, J.; Masion, A.; Borschneck, D.; Hazemann, J. L.; Macary, H. S.; Bottero, J. Y. New combination of EXAFS spectroscopy and density fractionation for the speciation of chromium within an Andosol. *Environ. Sci. Technol.* **2006**, *40*, 7602−7608.
(20) Xiao-Quan, S.; Bin, C. Evaluation of sequential extraction for speciation of trace metals in model soil containing natural minerals and humic acid. *Anal. Chem.* **1993**, *65*, 802−807.
(21) McBride, M. B. *Environmental Chemistry of Soils*; Oxford University Press: New York, 1994.

Received for review February 2, 2007. Revised manuscript received June 26, 2007. Accepted July 11, 2007.

ES070260H

SUPPORTING INFORMATION

Manuscript title

Assessing the origin and fate of Cr, Ni, Cu, Zn, Pb, and V in an industrial polluted soil by combined microspectroscopic techniques and bulk extraction methods

Authors: *Terzano R., Spagnuolo M., Vekemans B., De Nolf W., Janssens K., Falkenberg G., Fiore S., Ruggiero P.*

Number of pages: 9
Number of figures: 4
Number of tables: 2

Site description

The soil samples were collected in Val Basento, an industrial district located along the Basento River (Basilicata, Italy), on the orographic right side of the river, which cuts through Pliocene and Pleistocene fine grained marine sediments. The sampling site is located a few hundred meters from the stream banks, on a paleo-fluvial plain. The phreatic surface is, therefore, a few metres below the ground surface and its position varies on the river flow regime. The lithological makeup of the substratum is heterogeneous and it reflects the composition of the sedimentary successions outcropping along the upper course of Basento River: shales, clays, sands, sandstones and carbonates. Mineralogical composition of the substratum depends on the grain-size particles: clay fraction (< 2 μm) is composed mainly of illite-smectite mixed layers, quartz, calcite and kaolinite, and of minor amount of illite, feldspars, and chlorite; the coarser particles are composed of phyllosilicates, quartz, calcite and feldspars.

Sequential extractions procedures

Sequential extractions were carried out following a modified Tessier procedure (reference 14 in the main text and 1 below): exchangeable fraction (ammonium acetate 1 M, pH 7, 25°C, 2 h); acid-soluble fraction (ammonium acetate 1 M, pH 5, 25°C, 2 h); reducible fraction (hydroxylamine hydrochloride 0.04 M, pH 2, 96°C, 6 h); oxidizable fraction (hydrogen peroxide 30%, pH 2, 85°C, 2 h); residual (microwave assisted digestion with HNO_3, EPA Method 3051). The BCR scheme (15, main text) was also adopted: acid-soluble fraction (acetic acid, 0.11 M, 25°C); reducible fraction (hydroxylamine hydrochloride 0.5 M, HNO_3, 25°C, 16 h); oxidizable fraction (hydrogen peroxide 30%, pH 2, 85°C, 1 h × 2 times); residual (Aqua regia, reflux, 2 h).

References

(1) Ure, A.M. Single extraction schemes for soil analysis and related applications. *Sci. Total Environ.* **1996**, 178, 3-10.

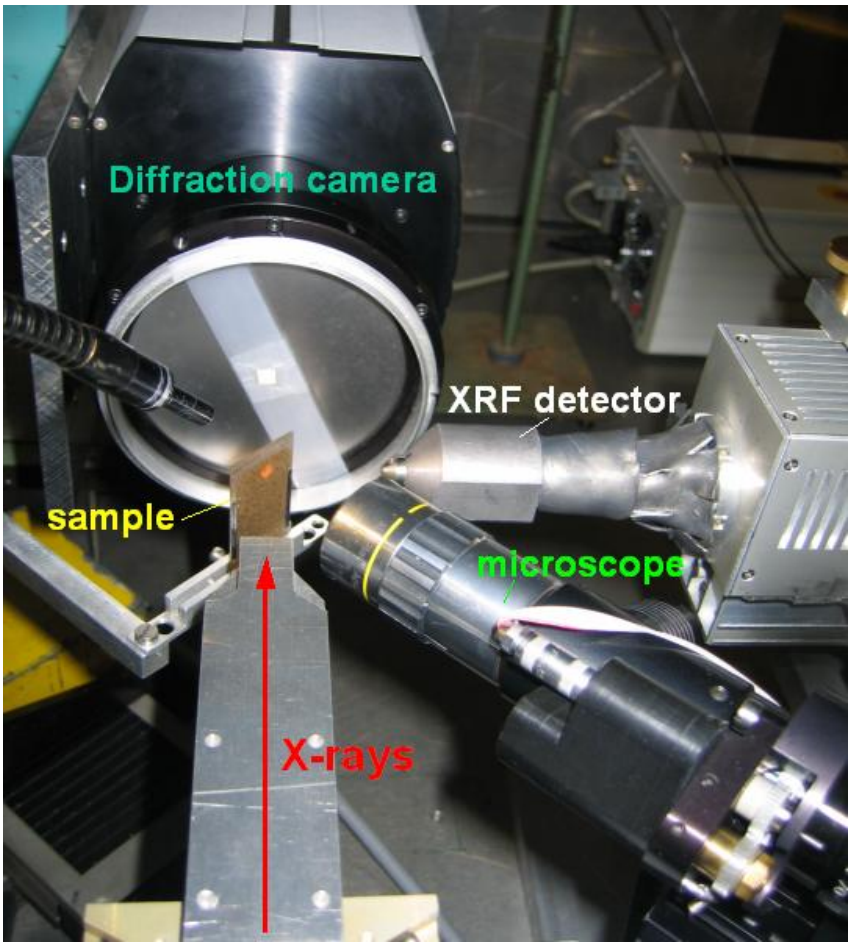

Figure S1. Experimental set-up adopted for combined μXRF/μXRD at Beamline L (HASYLAB – Hamburg, Germany).

Experimental details on the synchrotron X-ray microscopic analyses

Samples were placed on a motor x-y-z stage with a movement precision of 1 μm and set at an angle of 45° to the incident beam. Fluorescent radiation was collected with a Vortex-EX (Radiant Detection Technologies) Silicon Drift Detector with 50 mm^2 active area (1). Micro-diffraction patterns were collected in transmission mode on a Bruker SMART 1000 CCD detector with a detection area of 9 × 9 cm, and a pixel dimension of 61 μm in the 1k × 1k mode. Working in transmission configuration, μ-XRD and μ-XRF data can be simultaneously collected without modifying the sample orientation (2).

Several areas of the thin sections with dimensions of typically 500-800 μm horizontally and 300-700 μm vertically were previously selected and localized by SEM, as described in the text

(Materials and methods), for simultaneous μ-XRF and μ-XRD analyses. The employed 10-20 μm monochromatic X-ray beam of 19.311 or 24.024 keV was provided by a single bounce borosilicate glass capillary (3). 2D distribution maps were collected with 10-20 μm step size and dwell times of 40 sec per combined μ-XRF/μ-XRD measurements. The XRF spectra were evaluated using the AXIL software package (4), and the μ-XRD diffraction images and diffractograms were processed using Fit-2D (5) and XRDUA (6) software packages.

From the obtained microscopic XRF/XRD maps, points of interest could be selected in order to obtain additional information on Cr, V and Zn using the μ-XANES technique. The applied Si (1 1 1) double crystal monochromator had an energy resolution of ca. 0.8 eV and, in this case, a polycapillary lens (X-ray Optical System, Albany, NY) was used to produce a 20 μm analyzing X-ray beam. Pure foils of the elements of interest were scanned in order to perform the energy calibration, and three measurements were done on each selected sample and various Cr, V and Zn standard compounds [$Cr(NO_3)_3$, $Cr_2(SO_4)_3$, K_2CrO_4, Chromite, Cr(III) acetate, $CrCl_3 \cdot 6H_2O$, V_2O_3, VO_2, V_2O_5, Franklinite, $Zn_3(PO_4)_2$, ZnS, $ZnSO_4$, $ZnCl_2$, etc.]. The acquired XANES profiles were evaluated using the WINXAS 3.1 software package (7).

References

(1) Falkenberg, G. Characterization of a Radiant Vortex Silicon Multi-Cathode X-ray Spectrometer for (total reflection) X-ray fluorescence applications. *HASYLAB Annual Report* **2005**, 1123-1124. Available at: www-hasylab.desy.de/science/annual_reports/2005_report/part1/contrib/49/15255.pdf

(2) Manceau, A.; Marcus, M.A.; Tamura, N. Quantitative speciation of heavy metals in soils and sediments by synchrotron X-ray techniques. In *Applications of Synchrotron Radiation in Low-Temperature Geochemistry and Environmental Science*; Fenter, P., Sturchio, N.C., Eds.; Reviews in Mineralogy and Geochemistry; Mineralogical Society of America, Washington, DC, USA, Vol. 49, pp. 341-428, **2002**.

(3) Bilderback, D.H.; Huang, R. X-ray tests of microfocusing mono-capillary optic for protein crystallography. *Nucl. Instr. and Meth. A* **2001**, 467-468 (part II), 970-973.

(4) Vekemans, B.; Janssens, K.; Vincze, L.; Adams, F.; Van Espen, P. Analysis of X-ray spectra by iterative least squares (AXIL) – New developments, *X-Ray Spectrom.* **1994**, 23, 278-285.

(5) Hammersley, A. Fit2D V12.034 (ESRF), **2004.** Available at: www.esrf.fr/computing/scientific/FIT2D/index.html.

(6) De Nolf, W. XRDUA V 3.3.1.9, **2006**. Available at: http://xrdua.ua.ac.be/.

(7) Ressler, T. WinXAS: A XAS Data Analysis Program under MS Windows, *J. Synchrot. Radiat.* **1998**, 5, 118-122.

Table S1: Soil semi-quantitative mineralogical composition (% dry weight)

Total (<2mm)		**Clay fraction (<2μm)**	
Clays	traces	Il/Sm + Chl/Sm	9 %
Quartz	34 %	Il + Mic	3 %
K-feldspars	4 %	Kao	1 %
Plagioclase	4 %	Chl	1 %
Calcite	46 %	Quartz	16 %
Hem/Mag/Goet	12 %	Plagioclase	6 %
Gypsum	traces	Calcite	49 %
		Hem/Mag/Goet	15 %
		Gypsum	traces

Hem: hematite; Mag: magnetite; Goet: goethite; Il: illite; Sm: smectite; Chl: chlorite; Mic:micas; Kao: kaolinite

Notes: Details on the semi-quantitative mineralogical determination are reported in: Terzano, R.; Spagnuolo, M.; Medici, L.; Tateo, F.; Ruggiero, P. Zeolite synthesis from pre-treated coal fly ash in presence of soil as a tool for soil remediation. *App. Clay Sci.* **2005**, 29, 99-110.

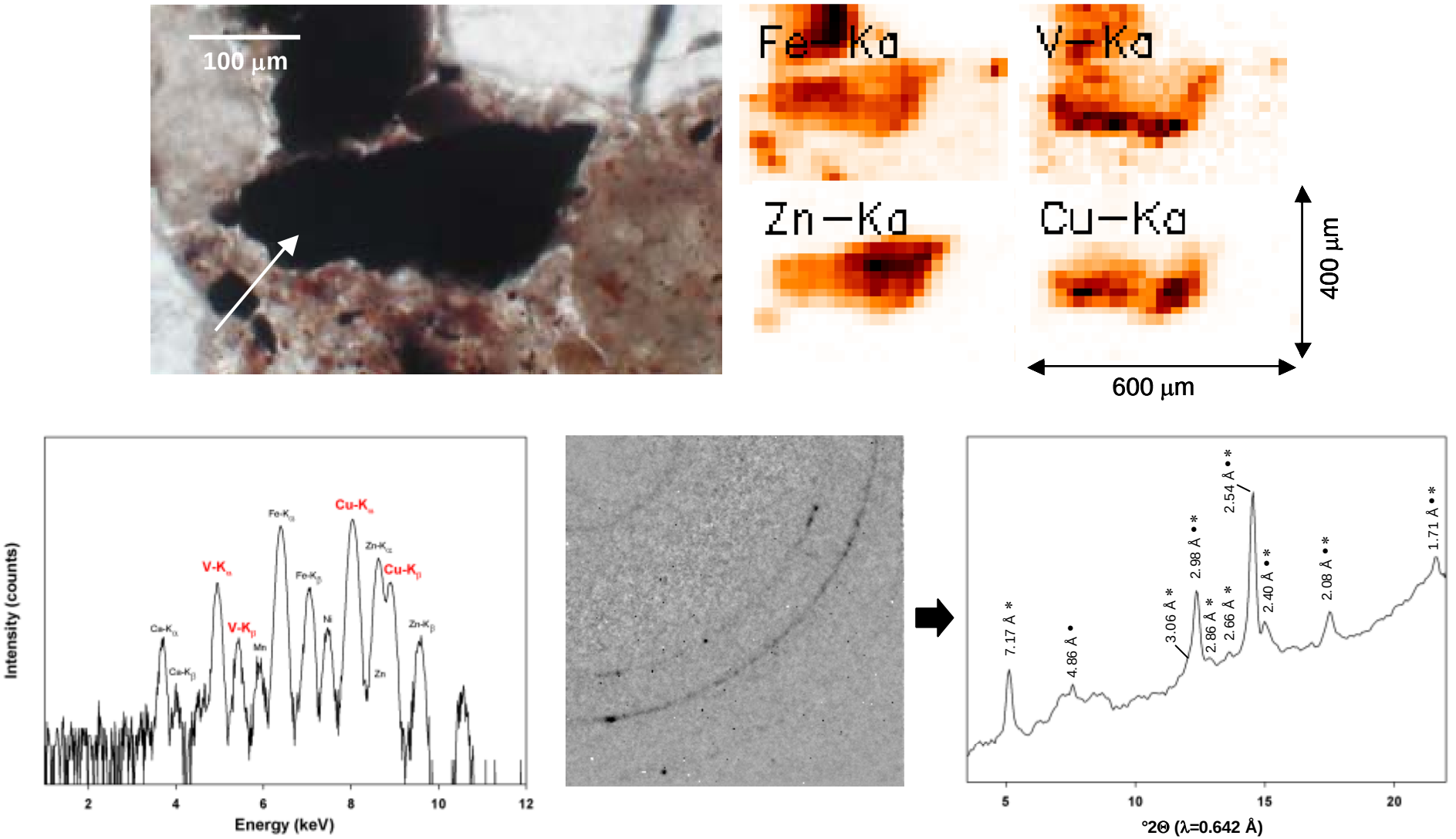

Figure S2: Micrograph with the corresponding µ-XRF distribution-maps (for Fe, V, Zn, and Cu) of a microscopic area on a soil thin section analysed by combined µ-XRF/µ-XRD. Darker pixels correspond to relative higher concentrations of the element. µ-XRF spectrum and µ-XRD image (also converted into 1D diffraction pattern) were collected in the point indicated by the arrow in the micrograph. The diffraction peaks of magnetite (•) and volborthite (∗) are indicated in the diffractogram.

Table S2: Attribution of the diffraction peaks reported in the diffractogram of Fig. 5 (main text). Diffraction data for minium, barite, lanarkite and crocoite are taken from MinCryst database (http://database.iem.ac.ru/mincryst/) and are relevant to diffraction patterns collected for powders of pure minerals. The uncertainty on peak attribution is within 2%. **λ=0.642 Å**.

Experimental diffraction peaks		**Minium**	**Barite**	**Lanarkite**	**Crocoite**
2teta (deg)	**d(Å)**	**d(Å) (h k l)**	**d(Å) (h k l)**	**d(Å) (h k l)**	**d(Å) (h k l)**
5.91	6.23	6.20 (1 1 0)		6.19 (2 0 0) 6.36 (0 0 1)	
6.60	5.58				5.51 (1 0 1)
8.53	4.32		4.33 (0 1 1)	4.43 (1 1 -1)	4.33 (2 0 0) 4.39 (0 1 1)
9.47	3.89		3.89 (1 1 1)		3.92 (1 1 1)
9.84	3.74			3.70 (2 0 1)	3.70 (2 0 1)
10.28	3.58	3.56 (0 2 1)	3.58 (0 0 2)		3.57 (0 0 2)
10.90	3.38	3.31 (1 2 1) 3.43 (2 1 1)	3.32 (1 0 2) 3.44 (2 1 0)	3.34 (3 1 0)	3.29 (1 0 2) 3.42 (2 1 0)
11.90	3.10	3.10 (2 2 0)	3.10 (2 1 1)		3.08 (2 1 1)
12.40	2.97			2.95 (4 0 -2) 2.96 (1 1 -2)	
12.71	2.90	2.86 (3 1 0) 2.90 (1 1 2)		2.85 (0 2 0) 2.86 (3 1 -2)	
13.21	2.79		2.83 (1 1 2)		2.79 (0 2 0) 2.83 (1 1 2)
13.65	2.70	2.69 (1 3 0)	2.72 (0 2 0)		2.75 (2 0 2)
14.02	2.63	2.59 (0 2 2) 2.66 (2 0 2)		2.60 (0 2 1) 2.60 (3 1 1)	
14.89	2.48		2.48 (2 1 2)		2.47 (2 1 2)
15.14	2.43	2.40 (2 3 0)		2.43 (2 0 2)	
16.02	2.30	2.31 (3 2 1)	2.32 (2 2 0)		
16.33	2.26	2.25 (2 2 2) 2.25 (2 3 1)		2.26 (2 2 1)	2.25 (3 0 2)
16.76	2.20		2.21 (2 2 1)		
17.51	2.11	2.09 (4 1 1)	2.10 (3 1 2) 2.10 (1 2 2) 2.12 (1 1 3) 2.12 (4 0 1)		2.07 (4 0 1) 2.08 (3 1 2) 2.12 (1 1 3) 2.13 (1 2 2)
18.20	2.03		2.05 (4 1 0)	2.05 (4 2 -2)	2.02 (4 1 0)
18.82	1.96	1.96 (1 4 1)		1.97 (6 0 -3)	1.96 (2 2 2)
19.32	1.91	1.90 (1 2 3)	1.93 (3 2 1)	1.91 (5 1 1)	1.93 (3 2 1)
19.95	1.85	1.87 (4 0 2)	1.85 (3 0 3)		1.85 (4 0 2)
20.25	1.83			1.84 (2 2 2) 1.84 (1 1 3)	1.83 (3 0 3)
21.07	1.76	1.75 (3 3 2) 1.77 (0 4 2)	1.75 (3 1 3) 1.75 (1 0 4) 1.76 (0 3 1)	1.74 (3 3 -1) 1.75 (6 2 -2) 1.74 (3 3 -1)	1.75 (4 1 2) 1.76 (1 3 1)
21.70	1.71		1.72 (1 3 1) 1.72 (5 0 1)	1.72 (3 3 0)	1.71 (2 3 0)

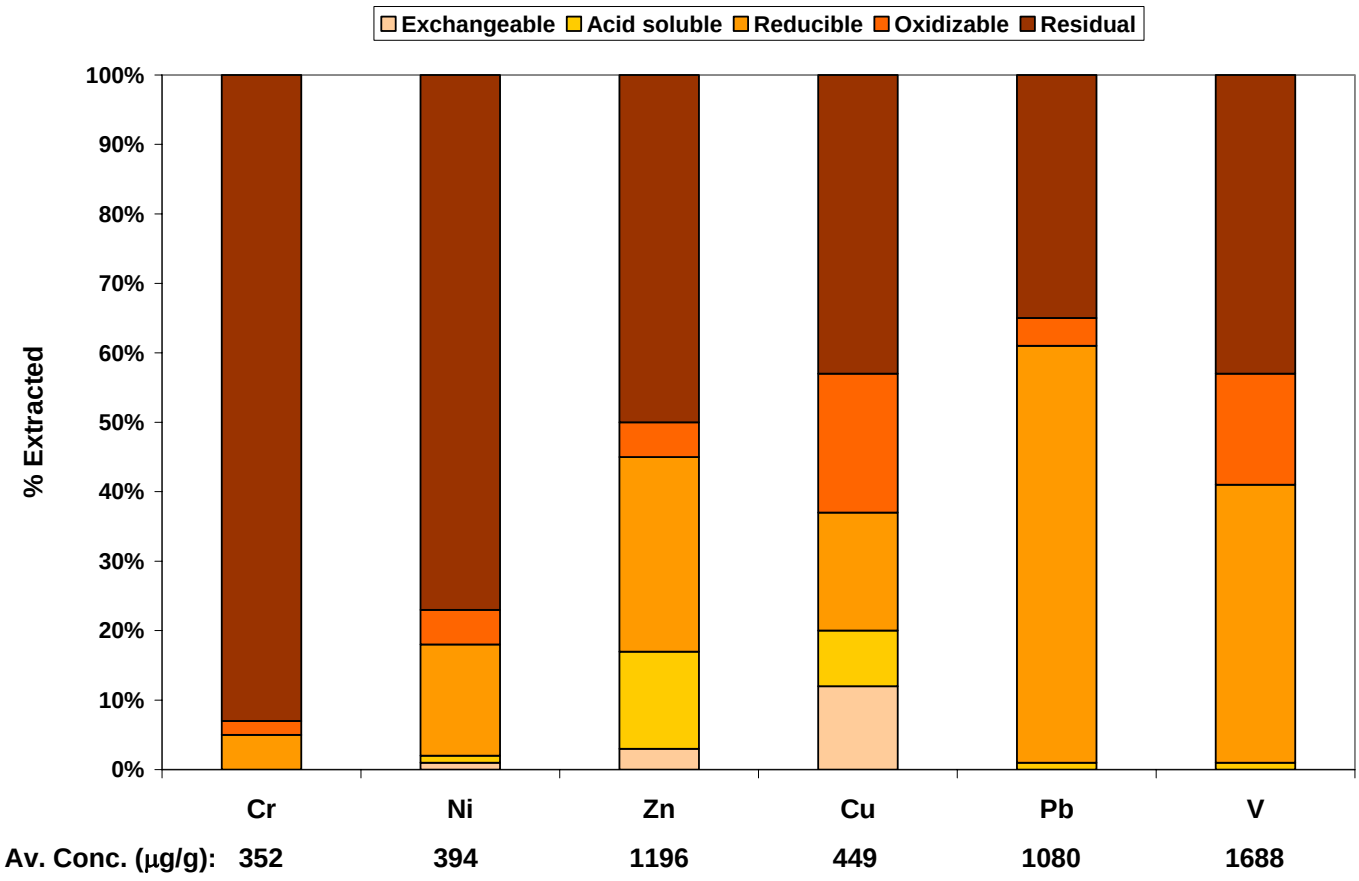

Figure S3: Results from the sequential extractions procedure and average metal content.

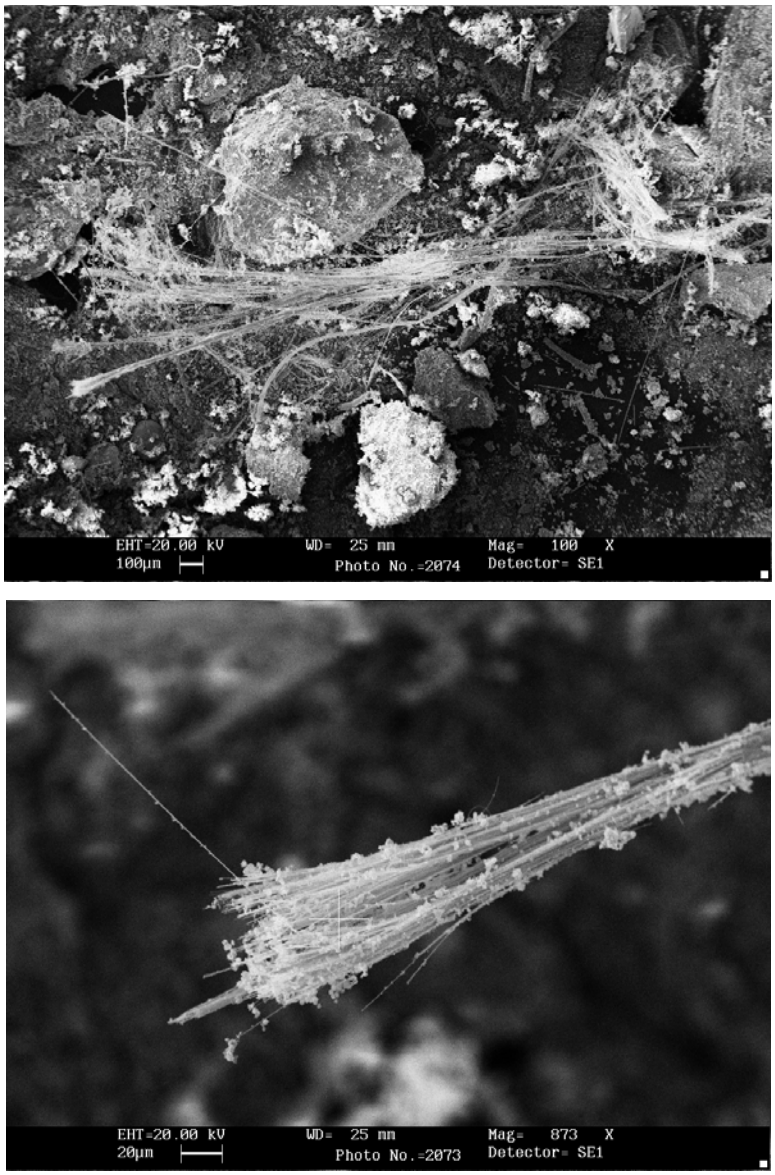

Figure S4: SEM micrographs of asbestos fibers found in the soil sample